Int. J. Electrochem. Sci., 13 **(2018)** 4276 – 4284, doi: 10.20964/2018.05.26

International Journal of
ELECTROCHEMICAL
SCIENCE
www.electrochemsci.org

3D Porous $LiNi_{0.5}Mn_{1.5}O_4$ with Improved Rate Capability and Cycle Stability

Shaoping Feng [1,2], *Xin Kong* [1,2], *Hongyan Sun* [1,2], *Baosen Wang* [1,2], *Tingbi Luo* [1,2], *Guiyang Liu*[1,2,*]

[1] Department of Chemistry, College of Science, Honghe University, Mengzi, 661199, Yunnan, China
[2] Local Characteristic Resource Utilization and New Materials Key Laboratory of Universities in Yunnan, Honghe University, Mengzi, 661199, Yunnan, China.
[*]E-mail: liuguiyang@tsinghua.org.cn

Received: 6 January 2018 / *Accepted:* 13 February 2018 / *Published:* 10 April 2018

A 3D porous $LiNi_{0.5}Mn_{1.5}O_4$ (3D-LNMO) was prepared by an easy cotton assisted solution combustion synthesis method. X-ray diffraction (XRD), infrared spectroscopy (FT-IR) and scanning electron microscopy (SEM) were used to characterize the phase structures and micro-morphologies of the products. Cyclic voltammetry (CV), electrochemical impedance spectroscopy (EIS) and galvanostatic charge-discharge testing were used to investigate the electrochemical performances. The results revealed that the as-synthesized $LiNi_{0.5}Mn_{1.5}O_4$ exhibited a 3D porous structure and ordered $P4_332$ space group. It showed significantly improved rate capability and cycle stability compared with the pristine $LiNi_{0.5}Mn_{1.5}O_4$ (P-LNMO) prepared without cotton under the same condition. The excellent electrochemical performances of 3D-LNMO might be attributed to its higher crystallinity and lower polarization.

Keywords: Porous $LiNi_{0.5}Mn_{1.5}O_4$; Lithium ion batteries; rate capability; cotton

1. INTRODUCTION

With the increasing application of electronic devices, lithium-ion batteries (LIBs) with high rate capability, high energy density and long cycle-life are required[1-4]. How to increase the rate capability of electrode materials without capacity decrease becomes a key issue needed to be solved. As the most promising cathode material, $LiNi_{0.5}Mn_{1.5}O_4$ has attracted much attention in recent years. Researches indicated that electrode materials with 3D porous structures generally have excellent rate capability[5, 6]. Cui et al [7] synthesized porous spinel $LiNi_{0.5}Mn_{1.5}O_4$ by microspheres $MnCO_3$ template method, and the product exhibited high rate capability and good cycle performance. Zhang et al [8] investigated porous spinel-type $LiNi_{0.5}Mn_{1.5}O_4$ with ordered $P4_332$ phase. The specific capacities of the fabricated $LiNi_{0.5}Mn_{1.5}O_4$ were 140 mAh/g at 1 C and 109 mAh/g at 20 C, and retained 91% at 5

C after 100 cycles. Pan et al [9] synthesized a porous $LiNi_{0.5}Mn_{1.5}O_4$ with a particular core-shell structure by template method. The specific discharge capacity of the as-prepared materials was 124.8mAh/g at 5C rate and retained 88.4% after 400 cycles. Yi et al [10] prepared porous spherical $LiNi_{0.5}Mn_{1.5}O_4$-CeO_2 with ordered $P4_332$ phase, and the products exhibited superior cycling stability, discharge capacity and rate capability. We have previously reported porous $LiNi_{0.5}Mn_{1.5}O_4$ prepared by a facile method with corn stalk or pine wood template[11, 12], and the products exhibited significantly improved electrochemical performance of cycling stability, specific capacity and rate capacity.

In this paper, a 3D porous $LiNi_{0.5}Mn_{1.5}O_4$ was synthesized by cotton assisted solution combustion method. The cotton which is used as template and fuel in the solution combustion system could be easily removed when treated at high temperature. The 3D porous $LiNi_{0.5}Mn_{1.5}O_4$ exhibits significantly improved rate capability and cycle stability compared with the pristine $LiNi_{0.5}Mn_{1.5}O_4$ because of the porous structure, low polarization and well crystallinity.

2. EXPERIMENTAL

2.1 Synthesis

Firstly, 10g mixtures of equal mole of CH_3COOLi and $LiNO_3$, $(CH_3COO)_2Ni$ and $Ni(NO_3)_2$, $(CH_3COO)_2Mn$ and $Mn(NO_3)_2$ with the ratio of 1.0:0.5:1.5 (in mole) were dissolved together in 15 ml distilled water until a settled solution was obtained. Then, moderate amount of cotton was soaked in the solution for 30 min. After filtrated, the sample was put into a furnace. The temperature of the furnace increased from 25 °C to 700 °C at a rate of 10 °C/min and maintained at 700 °C for 12h. After cooled down to 25 °C naturally, the desired $LiNi_{0.5}Mn_{1.5}O_4$ (3D-LNMO) was obtained. A pristine $LiNi_{0.5}Mn_{1.5}O_4$ (P-LNMO) was prepared for comparison under the same conditions without the use of cotton.

2.2 Characterization

XRD (X'pert pro, PANalytical), FT-IR (PerkinElmer, with KBr pellets) and SEM (Quanta FEG 250, FEI) were used to ascertain the phase structures and micro-morphologies of the as-synthesized 3D-LNMO and P-LNMO.

2.3 Electrochemical performance test

A CR2025 coin cell was assembled to measure the electrochemical performances of the products. The as-prepared $LiNi_{0.5}Mn_{1.5}O_4$ including 3D-LNMO and P-LNMO, Li metal foil, 1.0M $LiPF_6$ dissolved in EC/DMC (1:1 in weight), porous Celgard 2400 polyethylene membrane was used as cathode, anode, electrolyte and separator, respectively. For the preparation of the cathode electrode, a slurry of 80wt.% 3D-LNMO or P-LNMO, 10wt.% carbon black and 10wt.% PVDF which was dissolved in NMP was coated onto Al foil. The diameter of electrode is ~16 mm and $LiNi_{0.5}Mn_{1.5}O_4$ on

electrode is about 3.0 mg. After drying at 120°C for 12h in vacuum of the cathode electrodes, the cells (CR2050) were assembled in high purity Ar-filled glove-box and charged-discharged at a desired C rate (1C=150 mAh/g) between 3.5V and 5.0V.

The CV were performed at a scan rate from 0.05 to 0.25 mV/s during a voltage range from 3.5V to 5.0V using the electrochemical workstation (CHI 660). The EIS was measured using CHI 660 after charging to 5V of the cells. The amplitude of ac voltage was 5mV and the frequency was in the range of 0.1Hz-100 kHz.

3. RESULTS AND DISCUSSION

3.1 Phase composition

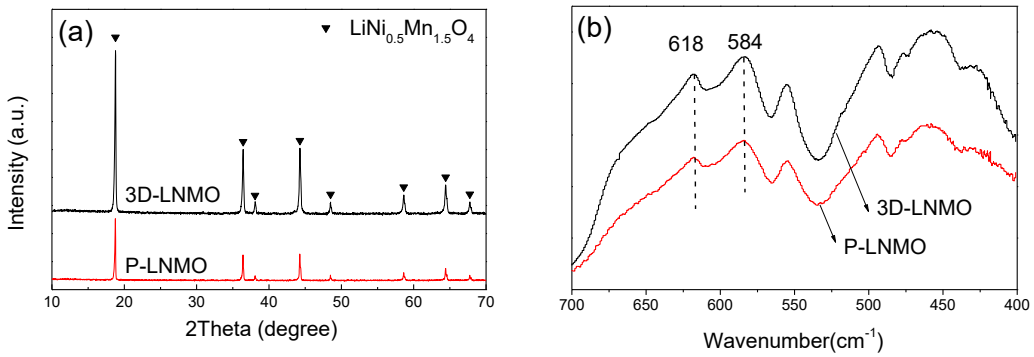

Figure 1. XRD patterns (a) and FT-IR spectra (b) of 3D-LNMO and P-LNMO.

The XRD patterns of 3D-LNMO and P-LNMO are shown in Fig.1 (a). All peaks of 3D-LNMO and P-LNMO correspond to $LiNi_{0.5}Mn_{1.5}O_4$, indicating that the two products are single phase $LiNi_{0.5}Mn_{1.5}O_4$. $LiNi_{0.5}Mn_{1.5}O_4$ spinel has two particular types of lattice structures, which are the ordered $P4_332$ and disordered Fd-3m[13, 14]. Generally, the $LiNi_{0.5}Mn_{1.5}O_4$ materials are the combinations of the two structures[15]. However, XRD analysis is difficult to be distinguish the difference between the ordered and the disordered structures[16]. FT-IR spectroscopy is an efficient technique to differentiate the ordering degree of the $LiNi_{0.5}Mn_{1.5}O_4$[17]. Fig. 1(b) shows the FT-IR spectra of 3D-LNMO and P-LNMO. The intensities of the Ni-O band at 584 cm^{-1} of the two products are stronger than those of the Mn-O band at 618 cm^{-1}, suggesting that the ordered structure in both 3D-LNMO and P-LNMO are dominant[18-20].

3.2 Morphology

Fig. 2 shows the SEM images of 3D-LNMO (a-d) and P-LNMO (e-f). As shown in Fig. 2(a)-(d), the numerous pores have been formed obviously within the whole 3D-LNMO material. The micro-morphologies of 3D-LNMO present a 3D interconnected porous structure which is similar to the cotton. The particles are well-crystallized and dispersed, and they exhibits typical spinel octahedral

aspect. Differently, P-LNMO exhibits agglomerated bulk morphologies and imperfect crystallinity (as shown in Fig. 2(e) and Fig. 2(f)). These results imply that 3D-LNMO has well crystallinity relative to the P-LNMO.

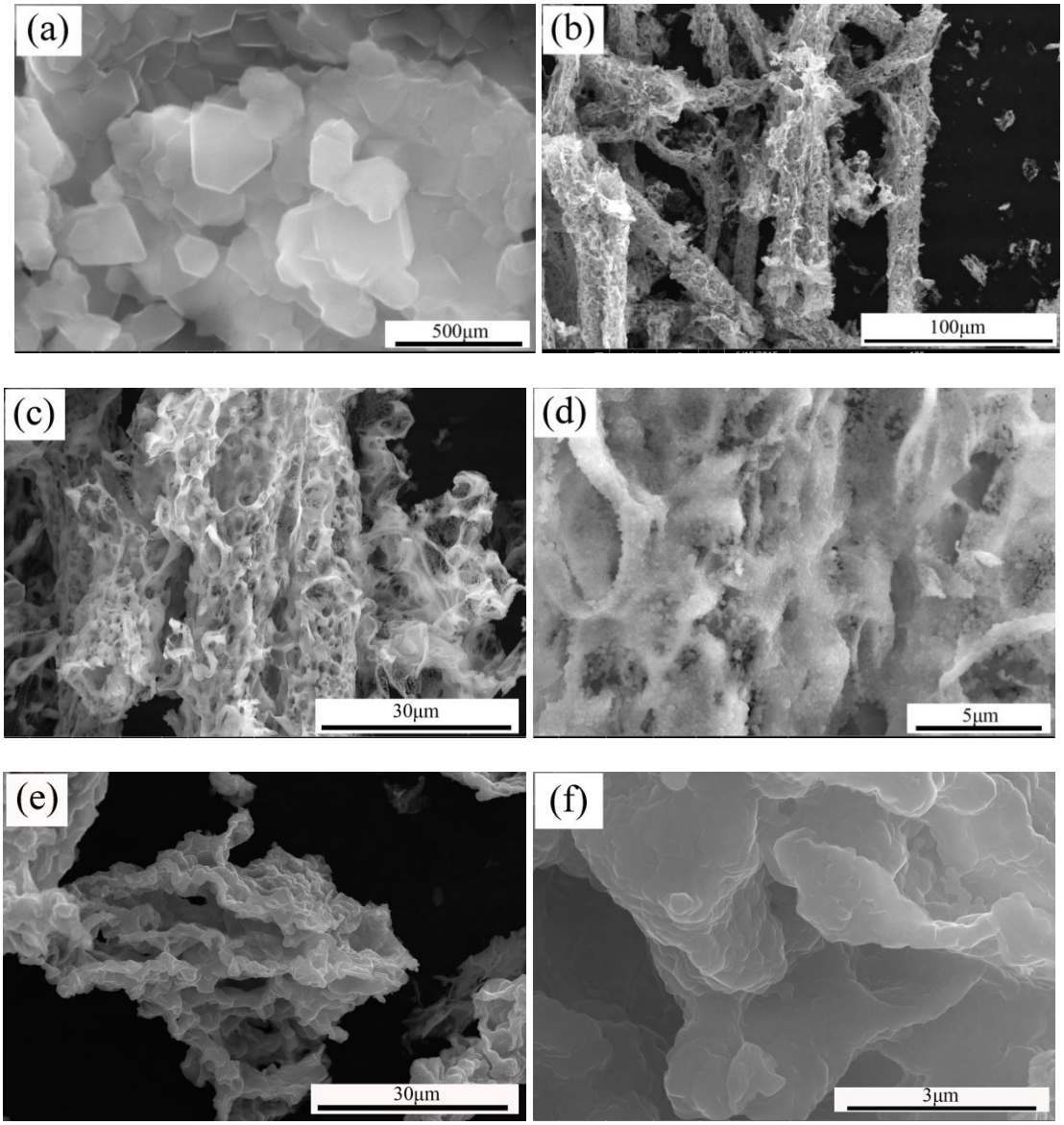

Figure 2. SEM images of 3D-LNMO(a-d) and P-LNMO(e-f)

3.3 Electrochemical performance

The initial charge-discharge curves of 3D-LNMO and P-LNMO are shown in Fig.3 (a). The initial capacities of charge and discharge of 3D-LNMO are 154.0 mAh/g and 128.9 mAh/g, respectively. The initial coulombic efficiency of 3D-LNMO is 83.7%. For P-LNMO, the initial capacities of charge and discharge are 150.3 mAh/g and 120.0 mAh/g, respectively, and the initial coulombic efficiency is 79.8%. The initial capacity and initial coulombic efficiency of 3D-LNMO are superior than these of P-LNMO. From Fig.3 (a) it also can be seen that the 4.0 V potential plateaus of

3D-LNMO and P-LNMO are very small, indicating that the two products have high degree of structural ordering[21], which are consistent with the results of FT-IR in Fig. 1(b).

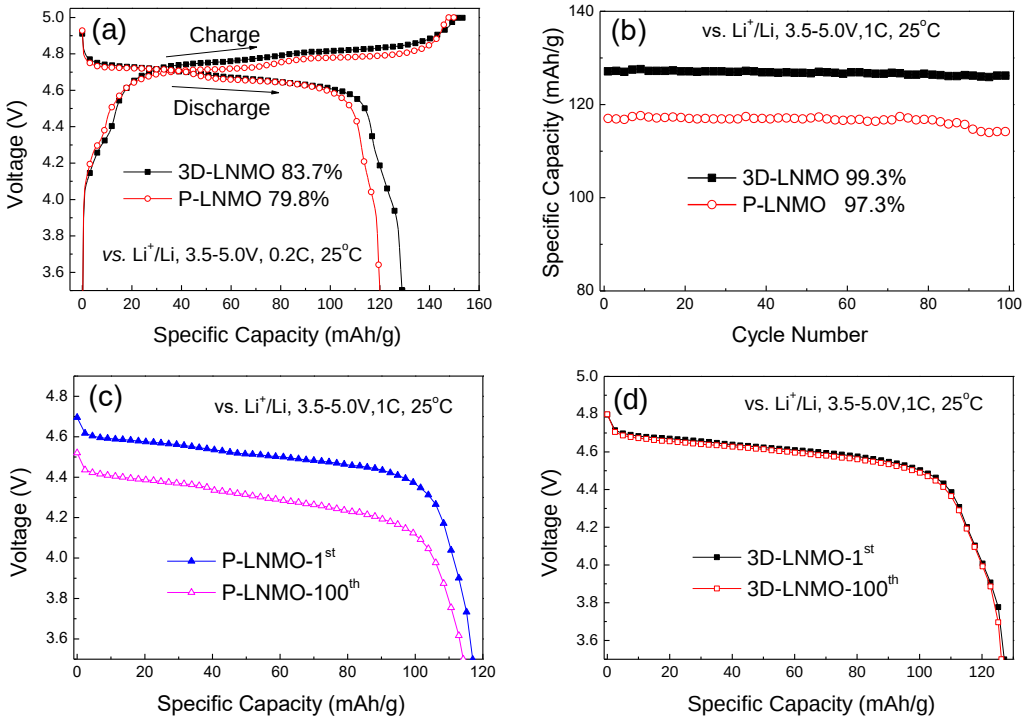

Figure 3. (a) The initial charge-discharge curves, (b) the cycling performances, (c) and (d) the discharge curves the first cycle and the 100th cycle of 3D-LNMO and P-LNMO.

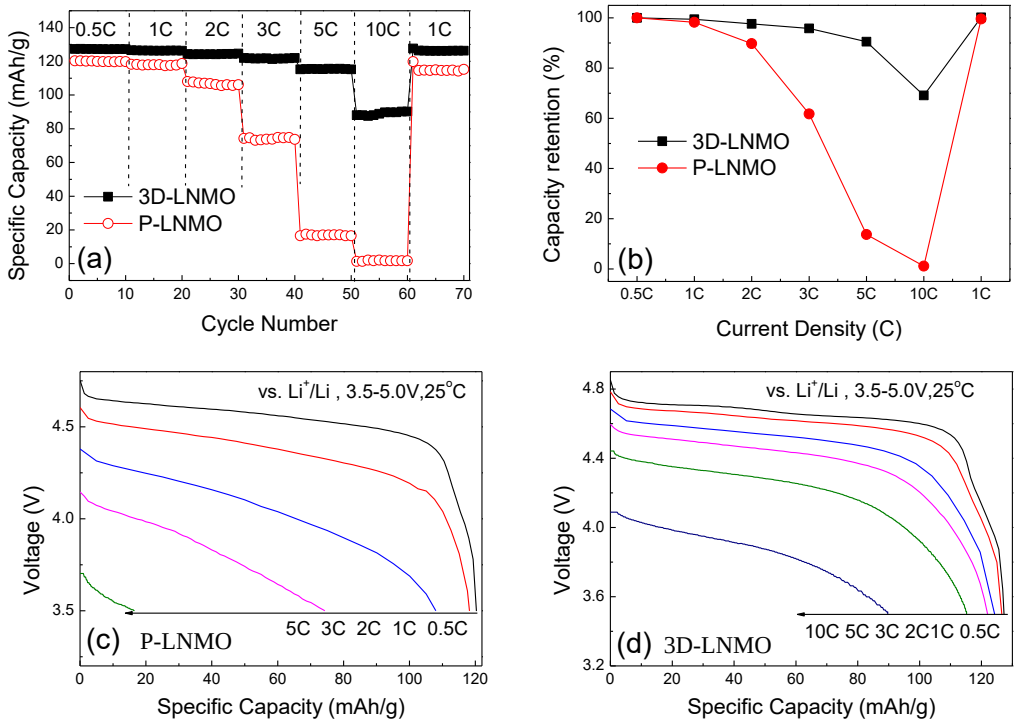

Figure 4. The rate capabilities (a), the capacity retentions (b) and the discharge curves at various C rates (c) and (d) of P-LNMO and 3D-LNMO.

The cycling performances of 3D-LNMO and P-LNMO at 25 ^{o}C are shown in Fig.3 (b). Both the two products display excellent capacity retentions. The capacity retentions of 3D-LNMO and P-LNMO are 99.3% and 97.3% after 100 cycles, respectively. However, the plateau voltage of P-LNMO drops obviously from the first cycle to the 100th cycle (as shown in Fig. 3(c)). On the contrary, the capacity and the plateau voltage of the first cycle and the 100th cycle of 3D-LNMO are nearly the same (as shown in Fig. 3(d)), suggesting that 3D-LNMO is more stable than P-LNMO during cycling.

The rate capabilities of P-LNMO and 3D-LNMO are shown in Fig.4 (a) and Fig.4 (b). The rate capability of 3D-LNMO is significantly improved, especially at higher rate. Fig.4 (c) and Fig.4 (d) show the discharge curves of P-LNMO and 3D-LNMO at various C rates. It is clear that with the increasing C rate, the plateaus voltage of P-LNMO drop is much larger than that of 3D-LNMO. At 10C, 3D-LNMO can deliver the capacity of 88 mAh/g, but the capacity of P-LNMO at 10C nearly drops to 0 mAh/g. Moreover, compared with other cathode materials of $LiNi_{0.5}Mn_{1.5}O_4$-based spinels[22-26], the rate capability and cycling performance of 3D-LNMO are also superior(Table 1).

Table 1. Comparison of the rate capability and cycling performance at room temperature for the similar cathode materials with 3D-LNMO.

Sample	Rate capability (mAh/g)	Cycling performance (capacity retention/%)	Reference
$LiNi_{0.5}Mn_{1.5}O_4$	0, 10C	55.1%, 1C, 100th cycle	[22]
$LiNi_{0.5}Mn_{0.485}Si_{0.015}O_2$	75, 10C	78%, 1C, 100th cycle	[23]
$LiNi_{0.5}Mn_{1.5}O_4$	60, 10C	81.33%, 0.2C, 100th cycle	[24]
$LiMn_{1.45}Cr_{0.1}Ni_{0.45}O_4$	40, 5C	98.3%, 0.2C, 125th cycle	[25]
$LiMg_{0.07}Ni_{0.43}Mn_{1.5}O_4$	74, 5C	-----	[26]
$LiNi_{0.5}Mn_{1.5}O_4$	88, 10C	99.3%, 1C, 100th cycle	This work

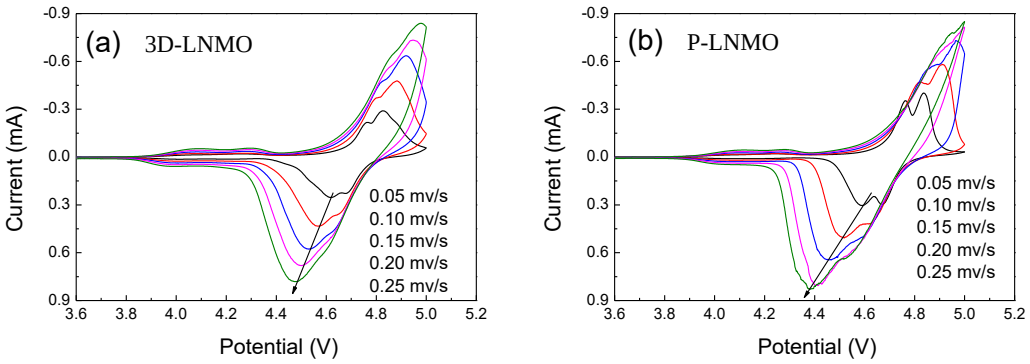

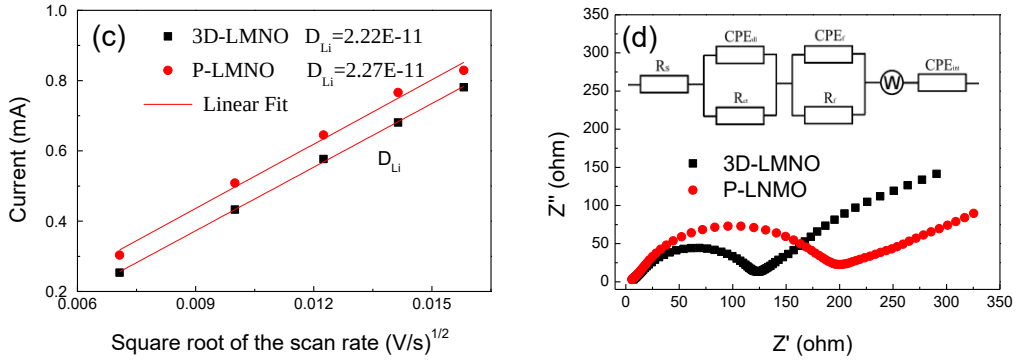

Figure 5. CV of 3D-LNMO (a) and P-LNMO (b) at various scan rates. (c) The plotting of peak current (i_p) vs. square root of the scan rate ($v^{1/2}$) for 3D-LNMO and P-LNMO. (d) EIS spectra of 3D-LNMO and (b) P-LNMO in 0.1Hz-100kHz range after 3rd cycles.

The electrochemical behavior of 3D-LNMO and P-LNMO were further investigated according to CV and EIS. As seen from Fig. 5(a) and Fig. 5(b), two oxidation/reduction peaks around 4.7V and 4.0V exist in both 3D-LNMO and P-LNMO products, which are associated with the $Ni^{2+}/Ni^{3+}/Ni^{4+}$ and Mn^{3+}/Mn^{4+}, respectively[27,28]. This is consistent with the charge and discharge curves in Fig. 3. Meanwhile, the peak shape change of 3D-LNMO is smaller than that of P-LNMO with the increasing of scanning rate from 0.05 to 0.25 mV/s. It means that 3D-LNMO has a lower polarization compared with P-LNMO. Furthermore, the weak peak at around 4.0 V indicates that few Mn^{3+} ions were present in 3D-LNMO and P-LNMO[29].

Fig. 5(c) shows the i_p vs. $v^{1/2}$ of 3D-LNMO and P-LNMO and the lithium-ion diffusion coefficient (D_{Li}) of them has been calculated from Equation(1)[30, 31].

$$i_p = 2.69\times10^5 n^{\frac{3}{2}} A C_{Li} D_{Li}^{\frac{1}{2}} \upsilon^{\frac{1}{2}} \qquad (1)$$

Where n is the number of electrons per molecule involving in transfer reaction (n=1), A is the electrode area (A=2 cm^2) and C_{Li} is the bulk lithium ions concentration in the electrode (C_{Li}=2.378×10^{-2} mol/cm^3). The calculated D_{Li} values of 3D-LNMO and P-LNMO are 2.22×$10^{-11}$$cm^2$/s and 2.27×$10^{-11}$$cm^2$/s (as shown in Fig. 5(c)), respectively, which are in agreement with the literatures[32, 33].

The EIS of 3D-LNMO and P-LNMO after 3rd cycled and a possible equivalent circuit are shown in Fig. 5(d). The intercept at the Z' axis assigns to the electrolyte resistance (Rs), while the semicircle corresponds to the Li^+ migration resistance(Rf) and the charge transfer resistance (Rct)[24, 34]. As is present in Fig. 5(d), the Rct of 3D-LNMO is smaller than that of P-LNMO, implying that 3D-LNMO has a lower electrochemical polarization than P-LNMO. It is a possible reason that 3D-LNMO has superior rate capability than that of P-LNMO.

4. CONCLUSIONS

In the work, a 3D porous $LiNi_{0.5}Mn_{1.5}O_4$ (3D-LNMO) was prepared by an easy cotton assisted solution combustion synthesis method. The 3D-LNMO has well crystallinity relative to the pristine

$LiNi_{0.5}Mn_{1.5}O_4$ (P-LNMO). The 3D-LNMO and P-LNMO were dominant with ordered $P4_332$ space group, but 3D-LNMO showed significantly improved rate capability and cycle stability compared with the P-LNMO. The capacity and the plateau voltage of the first cycle and the 100^{th} cycle at 1C of 3D-LNMO change little, while the plateau voltage of P-LNMO drops obviously. Moreover, at 10C, the capacity of 3D-LNMO is 88 mAh/g, but the capacity of P-LNMO at 10C nearly drops to 0 mAh/g. The excellent electrochemical performances of 3D-LNMO might be attributed to its higher crystallinity and lower polarization.

ACKNOWLEDGEMENT
This work was supported by the National Natural Science Foundation of China (No. 51362012, No. 51662007 and No. U1602273) and the Key Construction Disciplines of Chemistry for Master Degree Program in Yunnan.

References

1. N.D. Rosedhi, N.H. Idris, M.M. Rahman, M.F.M. Din, J. Wang, *Electrochim. Acta*, 206 (2016) 374-380.
2. Z.M. Zou, Z.J. Li, H. Zhang, X.H. Wang, C.H. Jiang, *J. Mater. Sci. Technol.*, 33 (2017) 781-787.
3. L. Wang, D. Chen, J.F. Wang, G.J. Liu, W. Wu, G.C Liang, *Powder Technology*, 292 (2016) 203-209.
4. L.G. Wang, F.Y. Li, Z. Min, *Int. J. Electrochem. Sci.*, (2016) 9941-9948.
5. Y. Li, L.Y. Cao, W.B. Li, L.L. Feng, J.F. Huang, J.Y. Li, *Mater. Lett.*, 214 (2018) 26-30.
6. J.Y. Liao, D. Higgins, G. Lui, V. Chabot, X.C. Xiao, Z.W. Chen, *Nano Lett.*, 13 (2013) 5467-5473.
7. Y.L. Cui, M.Z. Wang, J.L. Wang, Q.C. Zhuang, *Mater. Chem. Phys.*, 180 (2016) 46-52.
8. X.L. Zhang, F.Y. Cheng, J.G. Yang, J. Chen, *Nano Lett.*, 13 (2013) 2822-2825.
9. J. Pan, J.Q. Deng, Q.R. Yao, Y.J. Zou, Z.M. Wang, H.Y. Zhou, L.X. Sun, G.H. Rao, *J. Power Sources*, 288 (2015) 353-358.
10. T.F. Yi, X. Han, B. Chen, Y.R. Zhu, Y. Xie, *J. Alloys Compd.*, 703 (2017) 103-113.
11. G.Y. Liu, X. Kong, H.Y. Sun, B.S. Wang, Z.Z. Yi, Q.B. Wang, *Electrochim. Acta*, 141 (2014) 141-148.
12. G.Y. Liu, Y.N. Li, B.S. Wang, *Mater. Lett.*, 139 (2015) 385-388.
13. J.G. Yang, X.L. Zhang, Z.Q. Zhu, F.Y. Cheng, J. Chen, *J. Electroanal. Chem.*, 688 (2013) 113-117.
14. J.H. Kim, S.T. Myung, C.S. Yoon, S.G. Kang, Y.K. Sun, *Chem. Mater*., 16 (2004) 906-914.
15. S. Patoux, L. Daniel, C. Bourbon, H. Lignier, C. Pagano, F. Le Cras, S. Jouanneau, S. Martinet, *J. Power Sources*, 189 (2009) 344-352.
16. H.S. Fang, L.P. Li, G.S. Li, *J. Power Sources*,167 (2007) 223-227.
17. S. Ivanova, E. Zhecheva, R. Stoyanova, D. Nihtianova, S. Wegner, P. Tzvetkova, S. Simova, *J. Phys. Chem. C*, 115 (2011) 25170-25182.
18. J. Chong, S.D. Xun, X.Y. Song, G. Liu, V.S. Battaglia, *Nano Energy*, 2 (2013) 283-293.
19. N. Amdouni, K. Zaghib, F. Gendron, A. Mauger, C.M. Julien, *Ionics*, 12 (2006) 117-126.
20. T.F. Yi, J. Mei, Y.R. Zhu, *J. Power Sources*, 316 (2016) 85-105.
21. J.G. Yang, X.P. Han, X.L. Zhang, F.Y. Cheng, J. Chen, *Nano Res.*, 6 (2013) 679-687.
22. T. Kozawa, T. Murakami, M. Naito, *J. Power Sources*, 320 (2016) 120-126.
23. J.K. Chen, X.H. Tan, H.Q. Liu, L.M. Guo, J.T. Zhang, Y. Jiang, J. Zhang, H.F. Wang, X.M. Feng, W.G. Chu, *Electrochim. Acta*, 228 (2017) 167-174.
24. Y.L. He, J. Zhang, Q. Li, Y. Hao, J.W. Yang, L.Z. Zhang, C.L. Wang, *J. Alloys Compd.*, 715 (2017) 304-310.

25. D. Liu, J. Hamel-Paquet, J. Trottier, F. Barray, V. Gariépy, P. Hovington, A. Guerfi, A. Mauger, C.M. Julien, J.B. Goodenough, K. Zaghib, *J. Power Sources*, 217 (2012) 400-406.
26. C. Locati, U. Lafont, L. Simonin, F. Ooms, E.M. Kelder, *J. Power Sources*, 174 (2007) 847-851.
27. Y.J. Gu, Y. Li, Y. B. Chen, H.Q. Liu, H. H. Zhou, H.F. Wang, Y.Q. Han, J. Zhang, *Int. J. Electrochem. Sci.*, 12(2017), 9523-9532.
28. E.Q. Zhao, L. Wei, Y.D. Guo, Y.J. Xu, W.C. Yan, D.Y. Sun, Y.C. Jin, *J. Alloys Compd.*, 695 (2017) 3393-3401.
29. K. Lee, G.J. Yang, Y. Kim, *Ceram. Int.* 43 (2017) 15510-15518.
30. J.G. Kim, M.S. Park, S.M. Hwang, Y.U. Heo, T. Liao, Z. Sun, J.H. Park, K.J. Kim, G. Jeong, Y.J. Kim, J.H. Kim, S.X. Dou, *ChemSusChem*, 7 (2014) 1451-1457.
31. W.Q. Xu, H.L. Bai, Q.L. Li, T. Feng, J.M. Guo, L. Feng, C. Su, B. Wei, X. Liu, *Int. J. Electrochem. Sci.*, 12 (2017) 9758-9773.
32. D. Wang, X.H. Li, Z.X. Wang, H.J. Guo, Y. Xu, Y.L. Fan, J.J. Ru, *Electrochim. Acta*, 188 (2016) 48-56.
33. Q.Y. Chen, C.Q. Du, D.Y. Qu, X.H. Zhang, Z.Y. Tang, *RSC Adv.*, 5 (2015) 75248-75253.
34. A.K. Haridas, C.S. Sharma, T.N. Rao, *Electrochim. Acta*, 212 (2016) 500-509.